Influence of Cell Reversals on Cr/a- Pre Coated VS Post Coated Metallic Bipolar Plates in Automotive PEMFC Systems

Marc-Vincent Müller[1,2]*, Jan Schwämmlein[1]

[1]cellcentric GmbH & Co. KG
[2]Insitute of Energy Technology, Faculty of Engineering, University Duisburg-Essen
*corresponding author: marc-vincent.mueller@cellcentric.net

Fuel cells for applications in the transport sector can experience damaging stresses due to increased anode potentials as a result of hydrogen depletion and the resulting cell reversal. First analyses shall give an evaluation of these extreme conditions on metallic bipolar plates with a carbon based coating applied post-forming/pre-forming. Compared to the use of the coating with Au, the cell voltage decrease over the course of the cell reversal experiments is almost identical with the coating Cr/a-C regardless of the fabrication sequence. At the end of the tests, the polarization curve of the Cr/a-C coating is significantly lower than that of the Au coating. This correlates with the resistances, but they are not increased to the same extent. Surface analyses show that changes occur in the Cr/a-C post- and pre-coating in the area of water accumulation, while the gold coating remains unchanged.

KEYWORDS: BIPOLAR PLATE, CARBON COATING, POST-COAT/PRE-COAT, CELL REVERSAL

1. INTRODUCTION

The polymer electrolyte membrane fuel cell (PEMFC) is one of the key technologies for achieving climate neutrality in the transportation sector. One of the main components of the fuel cell stack, which has to meet many requirements such as electrical conductivity or cooling, is the bipolar plate (BP) [Karimi et al., 2012]. Incorrect operation is a particular source of bipolar plate degradation, leading to a loss of fuel cell performance. Anode hydrogen starvation is a major degradation mechanism, resulting in a negative cell voltage, a so-called cell reversal, in which the necessary protons and electrons for the fuel cell reaction are no longer available. This process is associated with a significant increase of the anode potential that undergoes water electrolysis and carbon oxidation [Hong et al., 2016]. The carbon corrosion proceeds as follows:

$$C + 2H_2O \leftrightarrow CO_2 + 4H^+ + 4e^-, E^0 = 0.207\,V\ (vs\ SHE) \qquad (1)$$

$$C + H_2O \leftrightarrow CO + 2H^+ + 2e^-, E^0 = 0.518\,V\ (vs\ SHE) \qquad (2)$$

To enable a high electrical conductivity, long lifetime and to withstand such extreme conditions, different coatings are therefore used for BPs made of metallic base material [Frangini et al., 2011], [Tawfik et al., 2012]. Due to their low cost and high availability, carbon-based coatings are a very good alternative compared to durable noble metals [Ijaodola et al., 2018]. Potentiostatic and potentiodynamic cyclic voltammetry (CV) analyses have demonstrated that carbon coatings in various compositions, both with and without a metallic interlayer, exhibit increased corrosion resistance on stainless steel BP materials compared to many non-noble metallic coatings [Sun et al., 2013], [Yi et al., 2013], [Zhao et al., 2016]. In addition, the electrical conductivity improves both before and after corrosive exposure, which was modeled after the fuel cell environment.
Typically, the coating is applied to the BP after forming, which is called post-coat. In contrast,

a new approach is the so-called pre-coat process, in which the coating is applied directly to the coil material before forming takes place. This offers great economic potential, as a continuous process is possible and manufacturing steps can be reduced [Dur et al., 2014]. To investigate the influence of the BP manufacturing sequence post-coat and pre-coat on the properties and durability, only a few scientific publications have been published [Dur et al., 2011], [Dur et al., 2014], [Turan et al., 2012], [Turan et al., 2013]. Corrosion resistance may deteriorate due to the pre-coating process, while the effect on electrical conductivity after aging is less and it can even improve. Since investigations of carbon coatings with different production sequences (post-coat/pre-coat) have not yet been carried out under the real damage case of cell reversal, first analyses are to be carried out in this work. The coating Cr/a-C is used, which has a carbon coating based on graphite like carbon (GLC) with a chromium intermediate layer. BPs with this coating are exposed to the influence of a cell reversal cycle in short stack format and compared to BPs with the reference coating Au. In-situ (polarization curves, performance points, resistance measurements) and ex-situ (resistance measurements, surface analyses) analyses are carried out in order to be able to make a first statement about the durability of the Cr/a-C coating under cell reversal events and the influence of the manufacturing sequence.

2. MATERIAL AND METHODS

The materials and methods used have also been partially described in another publication by Müller et al. [Müller et al., 2022].

2.1. Test equipment and materials

The test station used for the measurements of the data presented here is custom built by the company MS2 and was operated current controlled, unless otherwise mentioned. Parameter control was performed via LabView. Humidification was performed by evaporation humidifiers, which are present on the anode and cathode side.
The BPs have a serpentine flow field with an active area of 300 cm^2 and the base material 316L was provided by Outokumpu Nirosta GmbH. The BP design has been presented in an earlier publication [Talke, 2017]. The Au coating was applied as a post-coat process after the metal forming of the BPs. The Cr/a-C coating was applied by physical vapor deposition (PVD) at elevated temperature (~300 °C) at the Fraunhofer Institute for Material and Beam Technology (IWS) in Dortmund. Depending on the configuration, the deposition was performed on the welded BPs (post-coat) or on the metal coil (pre-coat). The coating thickness of the Cr/a-C coatings is approximately 90-100 nm Cr and about 50-60 nm a-C. The thickness of the Au coating is estimated to be in the µm range. The BPs were assembled without pretreatment using two BPs and one membrane electrode assembly (MEA) for the single cell configuration.
For the MEA, a PFSA based membrane with a paper type gas diffusion layer (GDL) was used. In addition, the MEA is equipped with a reversal-tolerant anode (RTA), which produces oxygen in the event of hydrogen undersupply. The cell assembly was clamped with a compression bladder to 0.4 N/mm^2. The MEA was conditioned for 17 hours and 12 minutes at a current density of 1 A/cm^2, an inlet temperature (T) of 65 °C resulting in an outlet temperature of 69 °C and a relative humidity (RH) of 85 ± 5%.

2.2. Cell reversal cycle

Hydrogen starvation occurs predominantly when the anode channels of the BPs are blocked and thus sufficient supply cannot be ensured. Blockages can occur, for example, due to water accumulation in the inlet area or frozen water [Taniguchi et al., 2004]. The cell reversal cycle is intended to represent this realistic scenario of hydrogen depletion as it would be possible in a real driving process. The cell reversal cycle of Bentele et al., who developed it as a new characterization method for the anode catalyst, serves as an orientation [Bentele et al., 2021].
Each cycle has, after an open circuit voltage phase (OCV), a steady state phase at constant current. The cell reversal phases take place at two different current densities (0.2 A/cm^2 and 0.65 A/cm^2), where the current density is slowly increased in a short transition phase. Prior to cell reversal, the anode is always extensively purged with nitrogen to remove hydrogen. The gases pass through the humidifier during all cycle steps, resulting in an RH of 120%. The stack inlet temperature is constant at 40 °C.
The cycle steps are shown as an overview in Fig. 1.

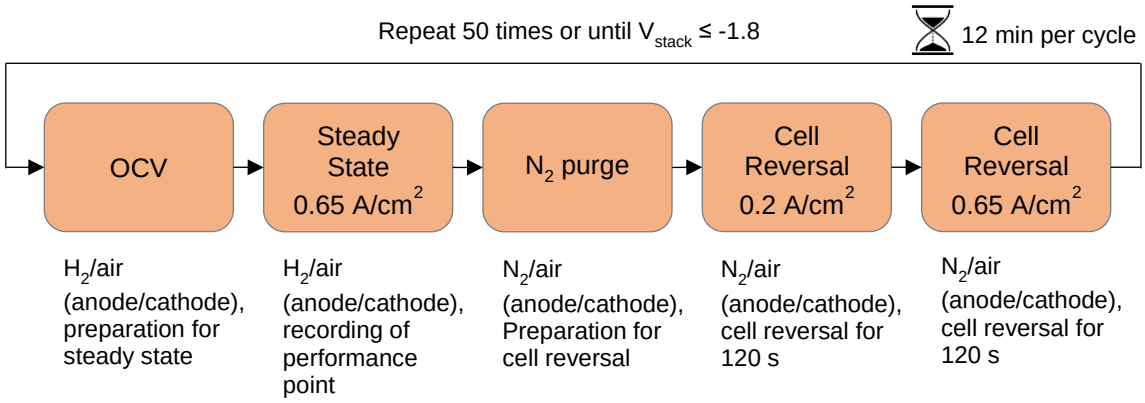

Fig. 1: Individual steps of the cell reversal cycle with short explanations of the individual cycle steps and conditions.

To prevent excessive degradation of the anode catalyst layer, the voltage cut-off criterion in the cell reversal phase was E ≤ -1.8 V_{stack}. Due to test bench limitations V_{stack} is used as termination criteria because the cell voltage monitoring and therefore V_{cell} cannot record voltages in this range.

2.3. In-situ analysis

Polarization curves and performance points were recorded to monitor the voltage progression. In addition, electrochemical impedance spectroscopy (EIS) measurements were performed by a Zahner IM6 potentiostat to determine the high-frequency resistance (HFR). All measurements were performed under H_2/air gas conditions. The conditions of the recordings are listed below in Table 1.

Table 1: Overview of conditions during recording of polarization curves, performance points and measurement by means of EIS.

Description	Current [A]	Current density [A/cm²]	Stoich-iometry/ flow rate	Inlet pressure [kPa$_{abs}$]	Inlet T [°C]	RH [%]	Recording frequency
Polarization curves	360-0 in nine steps	1.2 to OCV in nine steps	2/2 (anode/ cathode)	221.3/201.3 (anode/ cathode)	65	70 ± 12 85 ± 5 (anode/ cathode)	after every 50 reversal cycle
Performance points	195	0.65	2/2 (anode/ cathode)	151.3/131.3 (anode/ cathode)	40	120	after every reversal cycle
EIS	2 dc	-	3/6 l/min (anode/ cathode)	221.3/201.3 (anode/ cathode)	65	90	BOL/EOL

After the polarization curves were recorded, a ramp down phase over 92 min was performed in each case, during which T and RH were restored to the required conditions (40 °C, 120%) for the cell reversal experiments. The frequency range for the EIS measurements was between 100 mHz and 100 kHz at an amplitude of 0.1 A_{ac}.

2.4. Ex-situ analysis

For the ex-situ analyses on the BPs, the measurement of the interfacial contact resistance (ICR) and surface analyses by means of scanning electron microscope (SEM) and energy-dispersive x-ray spectroscopy (EDX) were used. The ICR measurements were performed using a self-built measuring device where the BP is placed between two gold-coated copper electrodes with GDL overlays, which are then pressed together with a constant pressure (0.38 N/mm²). The voltage drop between the electrodes and their surface area can then be used to determine the resistance. For each plate, 36 measurement points were recorded over the entire BP, with each measurement lasting 10 s. The measurements were made BOL and EOL for comparison.
To evaluate surface changes, SEM and EDX analyses were performed using a system from Tescan called MIRA 3 XMU. Sections of 2 x 2 cm² were cut out of the BPs. The material contrast was chosen as the mode for the images.

3. RESULTS AND DISCUSSION

3.1. Cell reversal induced voltage degradation

Polarization curves and performance points were recorded during the course of the cell reversal events to evaluate the voltage progression. First, the previously explained cell reversal cycle was applied to a cell with Au coated BPs as a reference. The results of the polarization curves BOL, after 50 cycles, after 100 cycles and EOL is shown in Fig. 2.

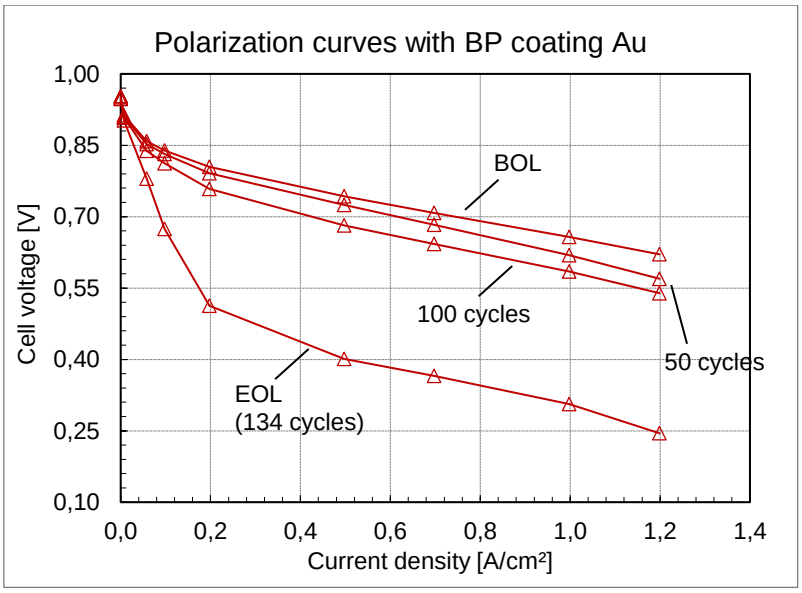

Fig. 2: Polarization curves when using Au coated BPs over the course of cell reversal cycles, conditions cell reversal: T_{inlet} 40 °C, RH 120%, conditions polarization curves: T_{inlet} 65 °C, RH_{anode} 70 ± 12%, $RH_{cathode}$ 85 ± 5%.

Thereby, after 50 and 100 cell reversal cycles at the maximum current density of 1.2 A/cm^2, there is a drop in cell voltage of 51 mV and 82 mV, respectively, compared to BOL, which corresponds to a drop of 8% and 13%. Noticeable is the sharp decrease of the polarization curve EOL, which was recorded after 134 cell reversal cycles, since here the termination criteria $V_{stack} \leq -1.8$ V was reached. At a current density of 1.2 A/cm^2, the voltage is 245 mV, which corresponds to a drop of 61% compared to BOL. The sharp drop in cell voltage can be explained by the fact that the anode catalyst is thinned out due to extensive carbon corrosion and the ohmic resistances increase as well as surface oxide formation takes place [Marić et al., 2020].

In order to evaluate the influence of cell reversal events of the carbon coatings and their fabrication sequence on the voltage profile, the experiments are also carried out in this case and polarization curves are recorded and compared with the results of the Au coated BPs. The results of the polarization curves BOL, after 100 cell reversal cycles and EOL using BPs with Cr/a-C post- and pre-coating and the comparison of the results with the Au coated BPs are shown below in Fig. 3.

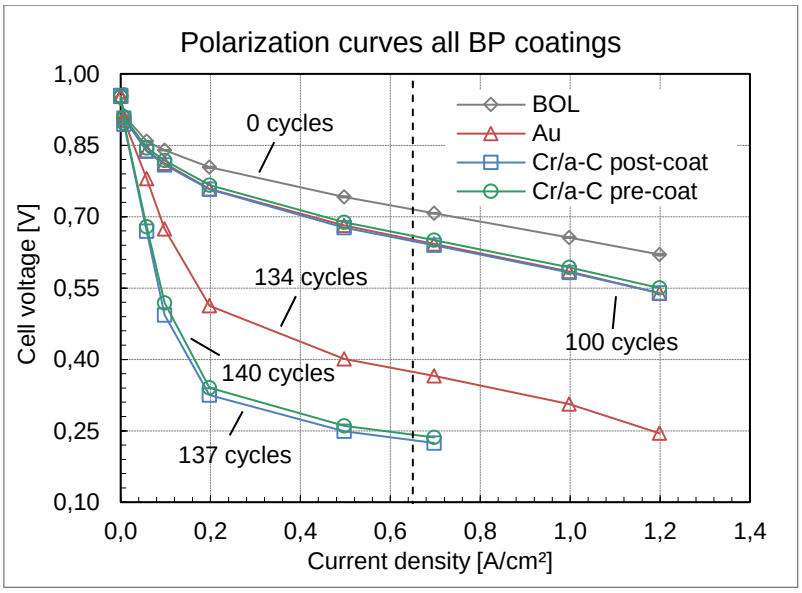

Fig. 3: Polarization curves BOL, after 100 cell reversal cycles and after the cut-off criterion is reached for the coating variations Au, Cr/a-C post-coat and Cr/a-C pre-coat, conditions cell reversal: T_{inlet} 40 °C, RH 120%, conditions polarization curves: T_{inlet} 65 °C, RH_{anode} 70 ± 12%, $RH_{cathode}$ 85 ± 5%.

All polarization curves BOL are plotted as average values with error bars indicating the minimal and maximal values. The vertical line in the graph shows that the performance points were recorded at this current density (0.65 A/cm^2). After 100 cell reversal cycles, the polarization curves are almost identical regardless of the coating and there is an average voltage drop of about 13% at a current density of 1.2 A/cm^2. Since there is hardly any difference in performance between the gold and carbon coatings up to this point, it is reasonable to assume that the voltage drop after 100 cycles is due to degradation of the catalyst surface area. The termination criteria for the cell reversal trials $V_{stack} \leq$ -1.8 V was reached after 134 cycles for Au, as previously mentioned. For Cr/a-C post- and pre-coat after 137 and 140 cycles. In this case, a significant drop in the voltages EOL occurs for the carbon coatings regardless of the fabrication sequence and only current densities up to 0.7 A/cm^2 can be achieved for the polarization curves compared to Au. The voltages at these current densities when using BPs with Cr/a-C post- and pre-coatings are 224 mV and 236 mV. Changes of the carbon coatings could lead to an increase in the resistances of the BPs and decrease of the performance. Another assumption is, that it is a measuring inaccuracy when the termination criteria is met. This briefly causes further degradation of the catalyst at high potentials, causing further performance degradation. This will be considered in more detail later on.

The recorded performance points, which were taken at a current density of 0.65 A/cm^2, can be seen in steps of five for all coating configurations in Fig. 4.

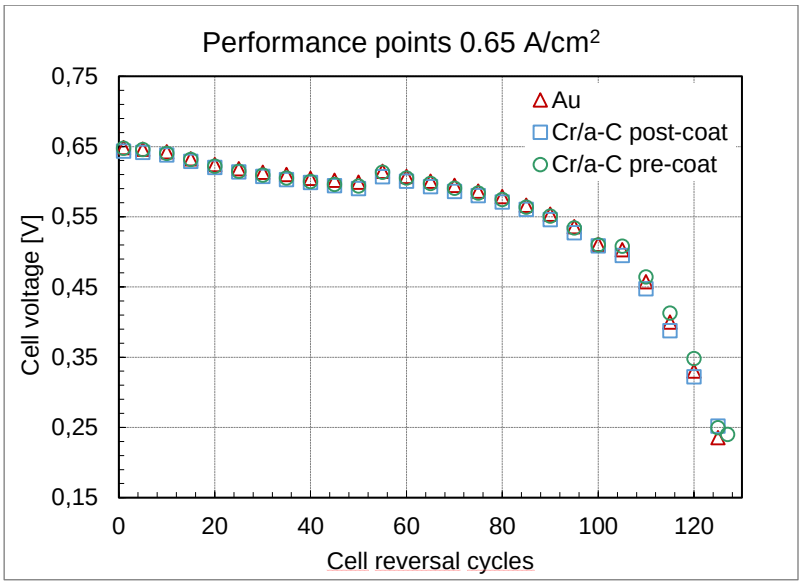

Fig. 4: Performance points after five cell reversal cycles each using the BP coating Au, Cr/a-C post-coat and Cr/a-C pre-coat, conditions cell reversal: T_{inlet} 40 °C, RH 120%, conditions performance points: T_{inlet} 40 °C, RH 120%.

In this case, recordings of up to 125-127 cell reversal cycles are possible before the required voltage can no longer be achieved. In general, the progression for all BP coatings used is very similar with only minor deviations. Up to 100 cycles there is only a moderate voltage decrease, before the decrease accelerates sharply and the voltage drops from about 510 mV to about 250 mV within 25-27 cycles. However, there is no noticeable impact of the coating type or manufacturing sequence on the voltage degradation at 0.65 A/cm². We assume that the slightly higher cell voltage of the performance points recorded directly after the polarization curves (55 and 105 cycles) results from a recovery effect caused by the polarization curve recording.

3.2. In-situ (HFR) and ex-situ (ICR) ohmic resistance measurements

The ohmic resistance measurement should show if there is a correlation between an increase in the resistances and the cell voltage loss and how this is influenced by the electrical conductivity of the BP. Therefore, in-situ measurements using EIS are a useful tool to obtain various information about the ohmic and mass transport resistances in the fuel cell over the course of the cell reversal tests. For each experiment, EIS measurements were performed immediately after the cell conditioning and after the cell reversal experiments. As an example, Fig. 5a shows the overview of the EIS analysis for the configuration with the BPs with the Cr/a-C pre-coating. Fig. 5b shows the detailed view of the intersection of the x-axis.

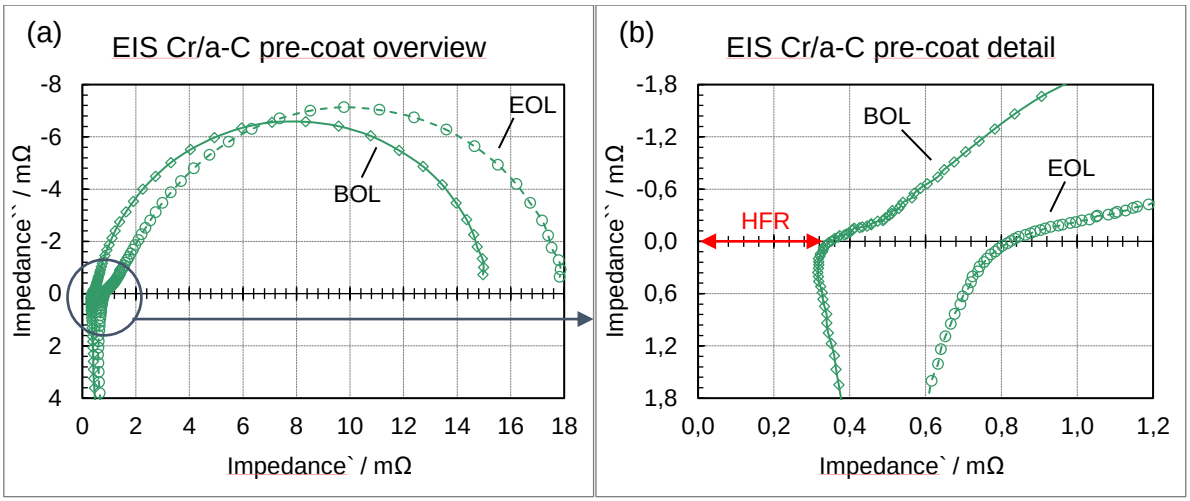

Fig. 5: Overview of the EIS measurements before and after the cell reversal tests (a) and detailed representation of the intersection of the x-axis to determine the HFR (b) exemplary for the BP coating Cr/a-C pre-coat, conditions EIS: T 65 °C, RH 90%.

At the point where the curve intersects the x-axis, the HFR can be determined. The HFR is composed of the resistance of the MEA and the contact resistance between MEA and BP. The ICR, on the other hand, is determined ex-situ by measuring the BPs at a total of 36 measuring points.
The results of the resistance measurements of the HFR and ICR for the BP coatings Au, Cr/a-C post- and pre-coat are shown in Fig. 6.

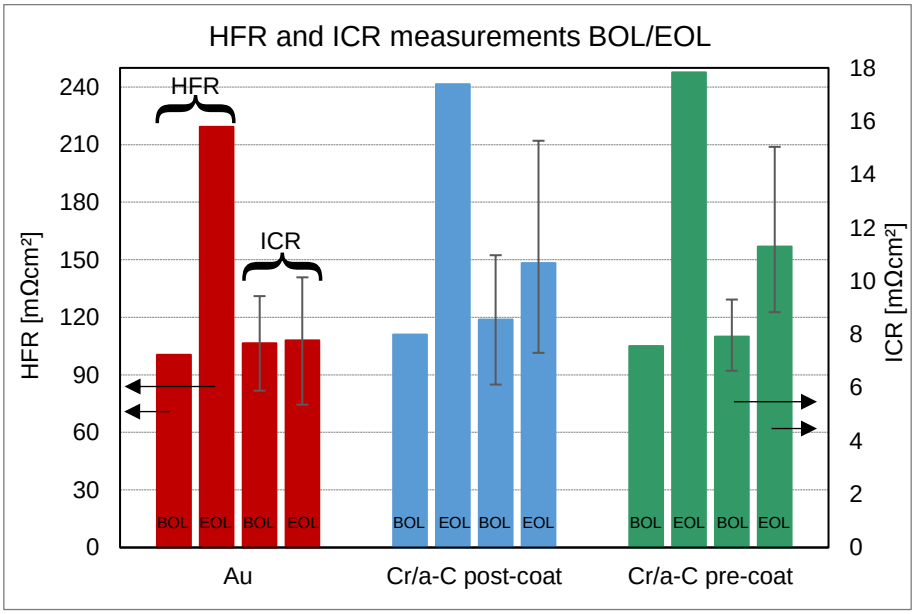

Fig. 6: Representation of the HFR determined by EIS in-situ measurements and the ICR determined by BP ex-situ measurements before and after the cell reversal tests for the coatings Au, Cr/a-C post- and pre-coat, for the ICR the average value of the 36 measuring points of two BPs per test is shown, the error bars indicate the average maximum and minimum deviations of all measuring points around the average value.

Looking at the HFR values after the tests, there is a significant increase of more than double the BOL value for all coating variants. The exact increases for the Au, Cr/a-C post-coat and Cr/a-C pre-coat coatings are 118%, 117% and 136%, respectively. This may either be related to the anode catalyst collapsing during the experiments, reducing the contact pressure of the BP on the MEA or/and to oxidation of the BP coating, resulting in an increased contact resistance. To discriminate the two effects, the HFR values can be compared to the ex-situ determined ICR values. As the ICR of the Au coated BPs remains constant from BOL (7.67 $m\Omega cm^2$) to EOL (7.77 $m\Omega cm^2$), we assume that the increase of the HFR of these cells is primarily caused by anode catalyst layer degradation and an associated loss of contact pressure on the MEA.
Since the value for the HFR when using the BPs with the carbon coating applied before forming is about 20% higher compared to the other coatings, this makes an influence of the fabrication sequence likely.
With the Au coating, the ICR BOL and EOL remain almost constant. This means that this coating has no influence on the increased HFR after the tests. The ICR behaves differently for the carbon coatings. Here, the values are 10.68 $m\Omega cm^2$ and 11.29 $m\Omega cm^2$ after the tests for Cr/a-C post-coat and Cr/a-C pre-coat, respectively, which corresponds to an increase of 25% and 43% compared to BOL. This suggests that changes in carbon coatings especially if they are applied before the forming process are occurring. The following SEM analyses should provide information on this.

3.3. SEM/EDX analysis of the BP surface

To examine the surfaces of the coated BPs, SEM and EDX analyses were carried out. When looking at the BPs with the Cr/a-C post- and pre-coat coatings after the cell reversal experiments, surface changes on the anode in the area of the first bend on the landings of the flow field are evident for both coating variations. In those areas water accumulation is expected. The gold coating was not examined more closely, as no changes were optically recognizable here. The images of the surface changes of the carbon coatings are shown in Fig. 7.

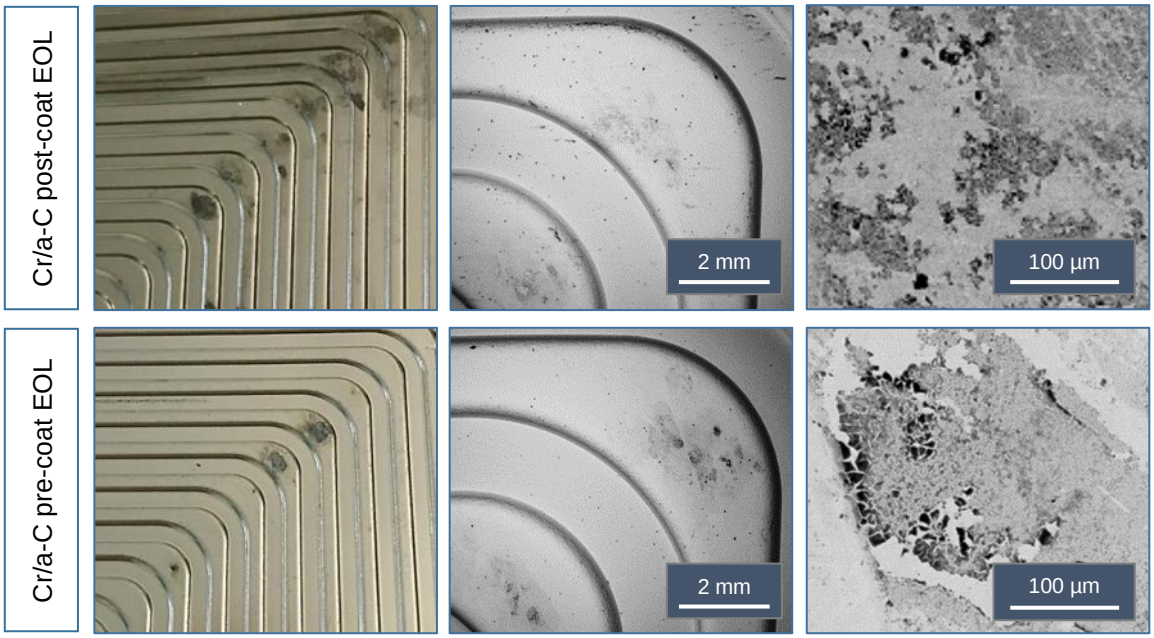

Fig. 7: Analyses of BP surfaces with Cr/a-C post- and pre-coating by SEM after cell reversal cycling.

It can be seen that there is dark staining in the altered surface areas, which is uneven. This could represent deposits or cracking of the coating. The dark areas are more pronounced in the pre-coat variant. Further analysis by EDX shows that there are high peaks of O in these areas for both coating variations after the tests. This suggests that oxidation processes may have occurred here. We assume that these surface alterations are responsible for the increase of the ICR that was discussed earlier. Unfortunately, no more precise statement can be made by EDX analysis as to whether and in what form the oxides are present. Further analyses are required to clarify how the coating has changed in the affected areas.

4. CONCLUSION

The results of the measurements presented in this manuscript show that none of the coatings has a significant impact on the performance degradation over the course of cell reversal cycling. However, for the EOL polarization curves, the voltage is significantly decreased for the carbon coatings compared to the Au coating. Further experiments should be performed here to determine if these are measurement inaccuracies or if the trend is confirmed. The BP coatings Cr/a-C also perform worse in the resistance measurements of the HFR and ICR, with the pre-coat variant having the highest values after the tests. The surface changes, which can be seen in the area of the BP bends, probably also have an influence here. These appear to be more distinct for the BP coating Cr/a-C pre-coat. Here, it should be analyzed in more detail how the surface changes and whether metal ions can emerge. The use of the BP coatings Cr/a-C post- and pre-coat offers a lot of potential, both economically and technically, but cannot be recommended without reservation, as further investigations are still required.

ACKNOWLEDGEMENTS

This work was supported by the German Federal Ministry of Economic Affairs and Energy [grant number 03ETB007C]. The funding project with the title miniBIP II was carried out by the cellcentric GmbH & Co. KG, Mercedes-Benz AG, Fraunhofer Institute for Material and Beam Technology (IWS) and Outokumpu Nirosta GmbH. The responsibility for the content of this publication lies with the authors.

REFERENCES

Karimi, S., Fraser, N., Roberts, B. and Foulkes, F. R. (2012) 'A review of metallic bipolar plates for proton exchange membrane fuel cells: Materials and fabrication methods', *Advances in Materials Science and Engineering*, 2012. doi: 10.1155/2012/828070.

Hong, B. K., Mandal, P., Oh, J. G. and Litster, S. (2016) 'On the impact of water activity on reversal tolerant fuel cell anode performance and durability', *Journal of Power Sources*, 328, pp. 280–288. doi: 10.1016/j.jpowsour.2016.07.002.

Frangini, S. and Zaza, F. (2011) 'Anti-Corrosion Methods for Fuel Cell Metal Bipolar Plates: A Review of Recent Patent Literature', *Recent Patents on Corrosion Sciencee*, 1(2), pp. 93–107. doi: 10.2174/2210683911101020093.

Tawfik, H., Hung, Y. and Mahajan, D. (2012) 'Bipolar Plate Durability and Challenges', in *Polymer Electrolyte Fuel Cell Degradation*. Elsevier Inc., pp. 249–291. doi: 10.1016/B978-0-12-386936-4.10005-3.

Ijaodola, O., Ogungbemi, E., Khatib, F. N., Wilberforce, T., Ramadan, M., El Hassan, Z., Thompson, J. and Olabi, A. G. (2018) 'Evaluating the effect of metal bipolar plate coating on the performance of proton exchange membrane fuel cells', *Energies*, 11(11). doi: 10.3390/en11113203.

Sun, H., Cooke, K., Eitzinger, G., Hamilton, P. and Pollet, B. (2013) 'Development of PVD coatings for PEMFC metallic bipolar plates', *Thin Solid Films*, 528, pp. 199–204. doi: 10.1016/j.tsf.2012.10.094.

Yi, P., Peng, L., Zhou, T., Wu, H. and Lai, X. (2013) 'Development and characterization of multilayered Cr-C/a-C:Cr film on 316L stainless steel as bipolar plates for proton exchange membrane fuel cells', *Journal of Power Sources*, 230, pp. 25–31. doi: 10.1016/j.jpowsour.2012.11.063.

Zhao, Y., Wei, L., Yi, P. and Peng, L. (2016) 'Influence of Cr-C film composition on electrical and corrosion properties of 316L stainless steel as bipolar plates for PEMFCs', *International Journal of Hydrogen Energy*, 41(2), pp. 1142–1150. doi: 10.1016/j.ijhydene.2015.10.047.

Dur, E., Cora, Ö. N. and Koç, M. (2014) 'Effect of manufacturing process sequence on the corrosion resistance characteristics of coated metallic bipolar plates', *Journal of Power Sources*, 246, pp. 788–799. doi: 10.1016/j.jpowsour.2013.08.036.

Dur, E., Cora, Ö. N. and Ko, M. (2011) 'Experimental investigations on the corrosion resistance characteristics of coated metallic bipolar plates for PEMFC', *International Journal*

of Hydrogen Energy, 36(12), pp. 7162–7173. doi: 10.1016/j.ijhydene.2011.03.014.

Turan, C., Cora, Ö. N. and Koç, M. (2012) 'Contact resistance characteristics of coated metallic bipolar plates for PEM fuel cells - Investigations on the effect of manufacturing', *International Journal of Hydrogen Energy*, 37(23), pp. 18187–18204. doi: 10.1016/j.ijhydene.2012.09.042.

Turan, C., Cora, Ö. N. and Koç, M. (2013) 'Investigation of the effects of process sequence on the contact resistance characteristics of coated metallic bipolar plates for polymer electrolyte membrane fuel cells', *Journal of Power Sources*, 243, pp. 925–934. doi: 10.1016/j.jpowsour.2013.05.182.

Müller, M.-V., Giorgio, M., Hausmann, P., Kinlechner, L., Heinzel, A. and Schwämmlein, J. (2022) 'Investigation of the effect of carbon post- vs pre-coated metallic bipolar plates for PEMFCs – start-up and shut-down', *International Journal of Hydrogen Energy*, 47(13), pp. 8532–8548. doi: 10.1016/j.ijhydene.2021.12.179.

Talke, A. K. (2017) *Der Einfluss von ausgewählten Luftschadstoffen auf die Brennstoffzelle unter fahrzeugnahen Betriebsbedingungen*. Universität Duisburg-Essen.

Taniguchi, A., Akita, T., Yasuda, K. and Miyazaki, Y. (2004) 'Analysis of electrocatalyst degradation in PEMFC caused by cell reversal during fuel starvation', *Journal of Power Sources*, 130(1–2), pp. 42–49. doi: 10.1016/j.jpowsour.2003.12.035.

Bentele, D., Aylar, K., Olsen, K., Klemm, E. and Eberhardt, S. H. (2021) 'PEMFC Anode Durability: Innovative Characterization Methods and Further Insights on OER Based Reversal Tolerance', *Journal of The Electrochemical Society*, 168(2), p. 024515. doi: 10.1149/1945-7111/abe50b.

Marić, R., Gebauer, C., Nesselberger, M. and Hasché, F. (2020) 'Towards a Harmonized Accelerated Stress Test Protocol for Fuel Starvation Induced Cell Reversal Events in PEM Fuel Cells : The Effect of Pulse Duration Towards a Harmonized Accelerated Stress Test Protocol for Fuel Starvation Induced Cell Reversal Events'. doi: 10.1149/1945-7111/abad68.